J. Indian Chem. Soc.,
Vol. 97, No. 9b, September 2020, pp. 1596-1603

Functionalization of silver nanoparticles with 1-naphthol-4-sulfonate for evaluation of ethylenediamine and diethylenetriamine

Subanti Das, Shaktibrata Roy, Nishithendu Bikash Nandi, Shamim Ahmed Khan, Moumita Majumdar and Tarun Kumar Misra*

Department of Chemistry, National Institute of Technology Agartala, Agartala-799 046, Tripura, India

E-mail: tkmisra70@yahoo.com, tkmisra.chem@nita.ac.in

Manuscript received online 30 June 2020, accepted 25 July 2020

Direct determination of polyamines (PAs) is an acute problem as PAs are not having any chromophoric or fluorophoric groups. Thus, a sensor is highly demanding to be developed for determining without derivatizing PAs from their aqueous solutions. In this context, functionalized metal nanoparticles (MNPs) having surface Plasmon resonance (SPR) band in the UV-Vis region could be the ultimate choice. Citrate stabilized spherical silver nanoparticle (cit-SNPs, d = 6.3 nm, σ = 1.23) were thus synthesized and functionalized with a photoacid, 1-naphthol-4-sulfonic (1Np4S) acid. The 1Np4S exhibits absorption maxima at 330 nm in water and pH > 7, which is the characteristic band of its anionic form. It shows two well defined excitation peaks (λ_{ex}) at 280 nm and 370 nm and an emission peak (λ_{em}) at 434 nm. Thus, 1Np4S is a fluorescent active species. In 1Np4S functionalized cit-SNPs, the fluorescent activity is ceased by the particles, because 1Np4S species get adsorbed onto the surface of cit-SNPs. The adsorption constant (K_{ad}) was determined using quenching phenomenon occurring at excitation and emission wavelengths of 1Np4S which is very high ranging, 6.23×10^{8}–16.47×10^{8} M^{-1}, indicating very strong interaction of the photoacid, 1Np4S with the cit-SNPs. The 1Np4S functionalized cit-SNPs were then used as nanoprobe for evaluating polyamines: ethylenediamine (EDA) and diethylenetriamine (DETA), as mimic of biogenic amines (BGAs). The calibration curves of EDA and DETA are straight lines with concentration ranges, (5.9–52.1 mM) and (3.9–50.6 mM), respectively. The result indicates that the sensitivity of evaluating DETA is higher than that of EDA.

Keywords: Silver nanoparticles, functionalization, adsorption constant, polyamines, fluorometric nanoprobe.

Introduction

Aliphatic polyamines are well known bioamines found in animals and plants and important analytical, medical, pesticides, dyestuffs and packaging reagents[1,2]. Generally, polyamines in low concentration are not considered toxic substances to individuals but of course in high concentration. The point of concern is their secondary role. They are prone to form nitrosated derivatives in the presence of nitrite or act as precursors for other compounds forming carcinogenic nitrosamines[3–5]. They are the cause of histamine-toxicity[6–9] as well. Moreover, ethylenediamine (EDA) and diethylenetriamine (DETA), the two simplest diamine and triamine, respectively are used as food additives or monomer in food packaging materials[2]. Their water solubility makes them environment contaminants. For example, EDA forms corrosive, toxic and irritating mist with the moisture in humid air, which may cause serious health damage[10]. EDA and DETA could be considered as mimic of biogenic diamines (putrescine (PUT), cadaverine (CAD)) and triamines (spermidine (SPD)) (Scheme 1). Biogenic amines (BGAs) are involuntarily present in foods[11] and food products. They trigger many physiological and toxicological effects on human health[11–13]. Thus, the development of methodology for evaluation of polyamines (PAs) from water media is remained challenging and demanding.

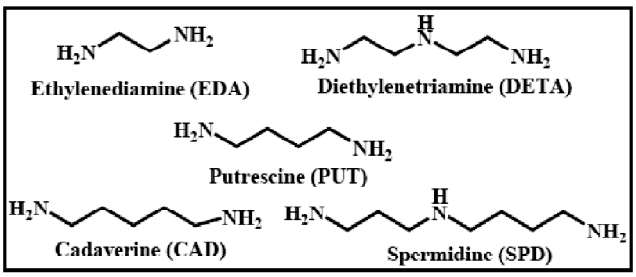

Scheme 1. Molecular structures of EDA and DETA and mimicking biogenic amines: putrescine (PUT), cadaverine (CAD), and spermidine (SPD).

Literature reveals that most of the studies have dealt with determination of polyamines based on HPLC separation followed by suitable derivatization of amines for detection either in fluorescence or UV-Vis techniques[14–26]. Paz-Pino *et al.* reported an HPLC method based on derivatization followed by determination of EDA[15]. Saito *et al.* method was a liquid chromatography with on-column fluorescence derivatization for determination of DETA in food samples[16]. However, Crea *et al.* reported a method based on high-performance ion exchange chromatography for the determination of both DETA and EDA in sea water[17]. In other way, Chen *et al.* developed a material based on lanthanide metal-organic frameworks for removing EDA from water[27].

In the field of nanosensors for cations, anions or neutral molecules, metal nanoparticles (MNPs), especially silver (Ag) and gold (Au) nanoparticles emerge as potential materials because of their surface Plasmon resonance (SPR) band in the visible range and tuning of such property in presence of analytes[28–32] lead to determination of analytes. However, functionalized MNPs as nanosensors for polyamines have scarcely been investigated. Chen *et al.* developed a method for the determination of aliphatic diamines based on Au-NPs[33]. Yao *et al.* used carboxyl-pillar[5]arene modified silver nanoparticles for successful discrimination of diamines[34]. Han *et al.* reported *p*-sulfonatocalix[6]arene modified Au-NPs as sensor for diaminobenzenes isomers[35]. Our investigation is to design a simple fluorescent probe based on silver nanoparticles (SNPs) for estimating EDA and DETA from their aqueous solution.

To make citrate stabilized SNPs (cit-SNPs) as a fluorescent probe for PAs, we have functionalized cit-SNPs with a photoacid, 1-naphthol-4-sulfonic (1Np4S) acid (Scheme 2). Förster, pioneer of photoacids, demonstrated that naphthols and their derivatives are photoacids[36–39]. They are considered to be weak acids in aqueous solution but become stronger acids (super acids) upon electronic excitation. For example, ground state pKa values of 1-naphthol and 2-naphthol are 9.2 and 9.5 whereas excited state pKa* values are 0.4 and 2.8, respectively[36].

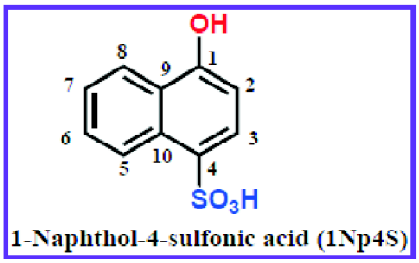

Scheme 2. Molecular structure of 1-naphthol-4-sulfonic acid.

Experimental

Materials and instruments:

All chemicals used in study were of analytical reagent grade and were used without further purification. Silver nitrate ($AgNO_3$), sodium borohydrate ($NaBH_4$), trisodium citrate ($Na_3C_6H_5O_7$), 1-napthol-4-sulphonic acid sodium salt ($C_{10}H_7NaO_4S$) were purchased from Merck and used as received. All solvents were of A.R. grade and used for preparation and spectroscopic studies. Standard methods were used to prepare universal buffer solutions. All the glassware were washed thoroughly with distilled water dried in an oven.

UV-Vis spectra were recorded on Shimadza UV-Vis 1800 spectrometer with a quartz cell of 1.0 cm path length. Dynamic light scattering (DLS) (microtrack Nanoflex W3463) was used to determine hydrodynamic particle size of nanoparticles. The surfaces of the particles were observed by Bruker, MultiMode-8 Atomic Microscope in tapping mode. Emission spectroscopy was studied on LS35 spectrofluorimeter (Perkin-Elmer). Transmission electron microscopy (TEM) (Technai G2 20 S-TWIN, electron microscope working at 200 kV) was used to determine particle size.

Preparation of citrate stabilized silver nanoparticles (cit-SNPs):

Citrate stabilized silver nanoparticles (cit-SNPs) were prepared following the reported sodium borohydrate ($NaBH_4$) reduction method[40]. Typically, 30 mL of sodium borohydrate solution (2.0 mM) was placed in a 100 mL beaker, which was then chilled in an ice bath. An aqueous solution of trisodium citrate (2 mL, 1% w/v) was added into the chilled $NaBH_4$ solution with continuously stirring. Finally, 10 mL silver nitrate solution (1 mM) was added into the reaction mixture drop by drop with stirring for 30 min. A bright yellow colored solution was formed which was stored in dark for further study.

Functionalization of cit-SNPs with 1-naphthol-4-sulphonic (1Np4S):

To functionalize cit-SNPs with the fluorophore, 1Np4S, a typical experiment was performed. An aqueous solution of 1Np4S (0.5 mL, 10 mM) was buffered to a pH 9.5. In keeping

the concentration of 1Np4S constant (1 mM), the concentration of cit-AgNPs was varied to a number of solutions (0.7–3.8 nM). These mixtures were shaken thoroughly at room temperature, settled for 10 min and recorded UV-Vis, excitation and emission spectra.

Evaluation of PAs using 1Np4S functionalized cit-SNPs :

In order to evaluate PAs, an aqueous solution containing fixed concentration of buffered 1Np4S (1 mM) and cit-SNPs (2.4 nM) was prepared. It was then treated with varying concentrations of EDA (5.9–52.1 mM) and immediately recorded UV-Vis, excitation and emission spectra.

For DETA, the same procedure was followed but the concentration range, 3.9–50.6 mM was maintained.

Results and discussion

Characterization of synthesized cit-SNPs:

Particles in nanometer range while preparing in bottom-up approach are prone to aggregate to bulk material. Thus, capping or stabilizing agent is required. Citrates are well known capping and reducing agents. In the present study we used citrate ions as a capping agent and $NaBH_4$ as a reducing agent. Thus, cit-SNPs were prepared by reducing aqueous Ag^+ ions with $NaBH_4$ to particles[40]. The as-formed particles are capped by the citrate ions, setting electrostatic barrier among particles and providing necessary stability to the particles. The cit-SNPs are well-dispersed in aqueous solution and are yellow in colour. The UV-Vis spectrum of the particles is shown in Fig. 1A. The particles show a strong absorption bands at 390 nm. The absorption bands of metal NPs, particularly those of the noble metals, are SPR bands that arise from the coherent oscillations of conduction electrons near the NP's surfaces, resulting in strong localized electric fields at its vicinity. When the frequency of coherent oscillation of surface Plasmon matches with the frequency of incident light, the absorption takes place to generate SPR band. Among the three metals that display Plasmon resonances in the visible spectrum (Ag, Au, Cu), Ag exhibits the highest efficiency of Plasmon excitation and it is the only material whose Plasmon resonance can be tuned to any wavelength in the visible and near infrared (NIR) range by modifying Ag NP's morphology (e.g. size and shape)[41], surface chemistry[42], the refractive index of the local environment[43], etc. The sudy of morphology of particles by AFM provides information about the surface aspects, especially shape of particles. cit-SNPs are spherical in nature; it could be understood from its AFM image in Fig. 1B. TEM image of cit-SNPs in Fig. 1C reveals that the particles are indeed spherical with diameter, 6.3 nm (σ = 1.23). The particles are well dispersed. The hydrodynamic size of the particles is about 34 nm and their size distribution can be understood

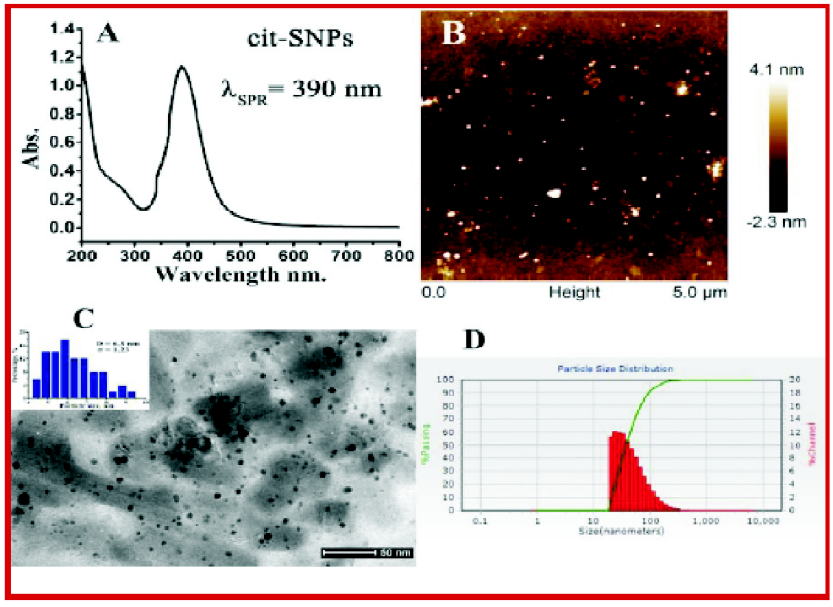

Fig. 1. cit-SNPs: (A) UV-Vis spectrum; (B) AFM topography; (C) TEM image (Insert, size distribution); (D) DLS size distribution.

from the DLS image, as shown in Fig. 1D.

Photophysical property of 1Np4S:

1-Naphthol-4-sulfonate (1Np4S) (Scheme 1) is a photoacid[37–39]. The absorption spectra of it in neutral water (pH 7), at pH 1.5 (adjusted with 1 *M* HCl) and at pH 12 (adjusted with 1 *M* NaOH) are shown in Fig. 2A. The 1Np4S shows an absorption maxima at 330 nm in water and at pH 12 but shifts to blue, at 295 nm at pH 1.5. It indicates that 1Np4S remains mostly in deprotonated form in water and at pH 12 as it has a pKa value of 8.27[44]. It gets protonated in acidic medium, pH 1.5; thus the absorption in this medium is due to its mostly neutral form (Fig. 2A).

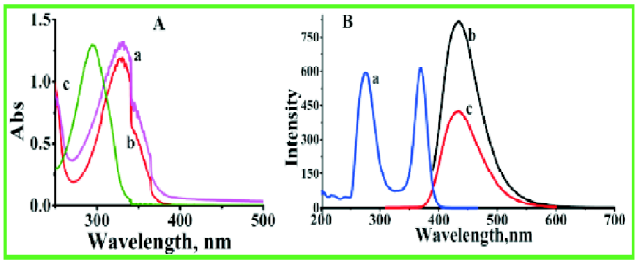

Fig. 2. (A) UV-Vis spectra of (a) 1Np4S in water (pH 7.0), (b) basic medium (pH 12) and (c) acidic medium (pH 1.5); (B) (a) excitation spectrum at λ_{em}, 480 nm and emission spectra at (b) λ_{ex}, 400 nm, (c) at λ_{ex}, 300 nm of 1-Np4S.

The excitation and emission spectra of 1Np4S is shown in Fig. 2B. 1Np4S shows two well defined almost equal intensity excitation peaks (λ_{ex}) at 280 nm (I = 594) and 370 nm (I = 608) at λ_{em}, 480 nm. It shows an emission peak (λ_{em}) at 434 nm for either excitation, λ_{ex} = 300 or 400 nm. 1-Naphthol and its derivatives stand out due to their extremely fast deprotonation rate[45–47]. 1Np4S in its first excited state behaves as a very strong acid with pKa* approaching zero[44]. As a result of the ultrafast deprotonation, in aqueous medium, the fluorescence intensity of the neutral form is extremely low and has not been observed for pH values as low as one. Therefore, it can be concluded that in aqueous media the observed emission is mainly due to the anionic form of 1Np4S.

Interaction of 1Np4S with cit-SNPs:

Determination of adsorption constant (K_{ad}):

Interaction of 1Np4S with cit-SNPs could be realised from the study of changing excitation and emission spectral intensities of 1Np4S in the presence of cit-SNPs. The excitation and emission spectra of 1Np4S in the presence of cit-SNPs are shown in Fig. 3. The data shown in Table S1 reveal that excitation intensities at λ_{ex} = 280 nm and λ_{ex} = 370 nm decrease gradually with increasing concentration of cit-SNPs (0.0–3.8 nM). The similar trend is observed in the emission data of 1Np4S at λ_{em} = 434 nm but the maximum red-shifts to 472 nm. These data were utilized for calculating adsorption constant of 1Np4S on the surfaces of cit-SNPs from Stern-Volmer (eq. (1)).

$$\frac{I_0}{I_x} = 1 + K_{ad}\,[\text{cit-SNPs}] \qquad (1)$$

where, I_0 is excitation or emission intensity of 1Np4S; I_x is excitation or emission intensity of 1Np4S in the presence of cit-SNPs; K_{ad} is the dynamic or static quenching constant which is supposed to be equivalent to adsorption constant of 1Np4S ions onto the surface of SNPs. The plots of $(I_0/I)_{ex/em}$ vs concentrations of cit-SNPs are shown in Fig. 4A. The curves show upward curvature, that is, towards y-axis after certain concentration of SNPs. Fluorescence quenching in between a fluorophore and a quencher may follow mainly two type of mechanisms: (i) Collisional or dynamic quenching. It suggests that the quencher comes in contact with the fluorophore and bring it down to the ground state without emission; (ii) Static quenching. The quencher forms complex/associates with the fluorophore in the ground state, which is non-fluorescence. Any of these two quenching processes leads the Stern-Volmer plots of the eq. (1) linear; which is used to determinate quenching constant. The present data plots (Fig. 4A) are linear upto certain concentration of the

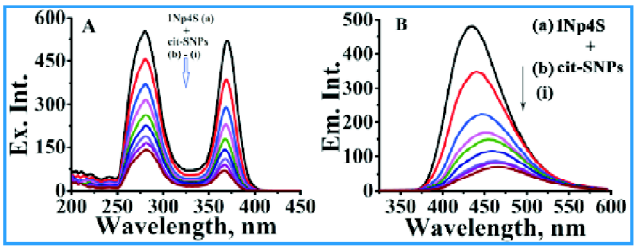

Fig. 3. (A) Excitation spectra of (a) 1-naphthol-4-sulfonic acid (1Np4S) at λ_{em}, 480 nm and (B) emission spectra of (a) 1-naphthol-4-sulfonic acid (1Np4S) at λ_{ex}, 300 nm where (b-i) 1Np4S in presence of cit-Ag-NPs (0.7–3.8 nM).

particles, indicating optimum concentration for leading dynamic or static quenching process. Further, increase of concentration may lead to complex mechanism, i.e. occurring both the mechanisms at a time. It may be the reason of co-existing of both the mechanisms[48–51]. In order to get known whether dynamic or static quenching occurs, the UV-Vis spectra of cit-SNPs in the presence of 1Np4S at different concentrations were recorded and are projected in Fig. 4B. As shown in Fig. 4B, the UV-Vis spectrum intensity at 330 nm of 1Np4S (Fig. 4B(a)) gets blue-shifted to 308 nm (Fig. 4B(d)) and the SPR band of the particles at 390 nm gets broadened, indicating ground state interaction of 1Np4S with the particles. The study thus confirms the static quenching process which makes 1Np4S quite non-fluorescent. Moreover, the highest concentration of the particles in the mixture leading static quenching is termed as the concentration of the particles for limit of linearity (LOL), which is found to be 2.8 nM in respect of emission quenching graph (Fig. 4A(c)). The SV plots (eq. (1)) upto LOL were performed for evaluating adsorption constant (K_{ad}); the data are given in Table S1. The K_{ad} value determined from the emission process (16.47×10^8 M^{-1}) is quite greater than that of the values from the excitation process (6.23×10^8 M^{-1} at λ_{ex} = 280 nm and 12.76×10^8 M^{-1} at λ_{ex} = 370 nm). Nevertheless, the high value of K_{ad} indicates very strong interaction of the photoacid, 1Np4S with the cit-SNPs.

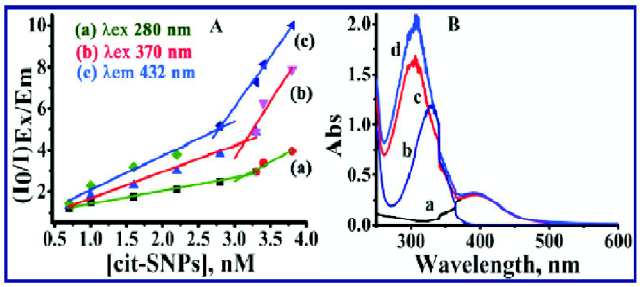

Fig. 4. (A) Stern-Volmer plots for the fluorophore, 1Np4S: (a) excitation band at 280 nm; (b) excitation band at 370 nm; (c) emission band at 432 nm in the presence of quencher cit-SNPs (0.7–3.83 nM); (B) UV-Vis spectra of (a) cit-SNPs (100 nM); (b) 1Np4S (concentration, 0.5 mM); (c) 'a' plus 1Np4S (conc. 0.2 mM); (d) 'a' plus 1Np4S (conc. 0.3 mM).

Evaluation of PAs:

The prime problem for direct detection of PAs, mimic of BGAs, lies in their structures as they have no chromophoric or fluorophoric moieties. We have therefore developed a nanoprobe, 1Np4S functionalized SNPs for spectro-fluorometric determination of PAs: EDA and DETA in buffered aqueous solution. The foregoing study helps us to construct the nanoprobe by mixing 1Np4S in a buffer solution of pH 9.5 with cit-SNPs of concentration, 2.4 nM, which is less than LOL, 2.8 nM (see Fig. 4A) to avoid complex quenching process. The developed nanoprobe was thus explored as potential sensor for quantification of EDA, and DETA.

Evaluation of EDA:

The evaluation of EDA concentration in aqueous solutions, a calibration curve of a plot of change of emission intensity (ΔI) vs concentration of EDA was constructed. The emission property of 1Np4S reversed back and its intensity gradually increased as EDA at various concentrations (5.9–52.1 mM) were added into the aqueous solutions of 1Np4S functionalized cit-SNPs (see Fig. 5A). The emission band position of 1Np4S functionalized cit-SNPs (24 nM) at 458 nm started blue-shifting to 434 nm (λ_{em} of 1Np4S) in the course of fluorometric titration. The phenomenon indicates that in the presence of EDA, the particles' surface adsorbed 1Np4S in its deprotonated form gets free from the surface gradually; as a consequence the emission of 1Np4S starts to reverse and increases gradually. In this context, it is reasonable to mention that the interaction of EDA with 1Np4S occurs through, perhaps, H-bonding and helps 1Np4S for desorption. It is worthy to mention that PAs are potential H-bond donors (-HNH/-NH- groups) whereas the deprotonated forms of 1Np4S could be considered as H-bond acceptors ($^-ONpSO_3^-$ groups). Thus, the H-bonded association in between 1Np4S and EDA may occur through $\cdots HNH\cdots {}^-ONpSO_3^-\cdots$ interactions. Calibration curve as constructed from a plot of change of emission intensity (ΔI) at 434 nm of 1Np4S functionalized cit-SNPs vs concentration of EDA is shown in Fig. 5B. The ΔI value increases lineraly with the concentration of EDA. The data are well fit in a linear equation, ΔI = 11.965 + 1.836 [EDA] with adj. R^2 = 0.99032. The slope (σ = 1.836) of the calibration and the standard deviation (s) of the blank assay data were used to evaluate the limit of detection (LOD = 3σ/s = 2.42 mM) and limit of quantification (LOQ = 10σ/s = 8.07 mM) for EDA. All data are listed in Table S2.

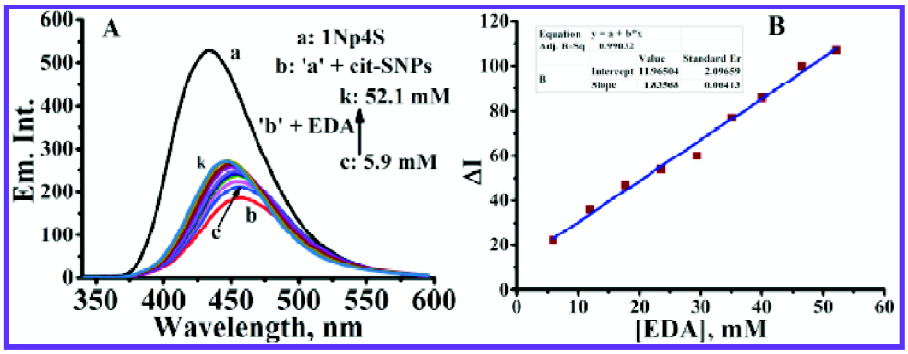

Fig. 5. (A) Emission spectra of (a) 1Np4S; (b) 'a' + cit-SNPs; (c-r) 'b' + EDA (5.9–52.1 mM); (B) calibration curve for EDA.

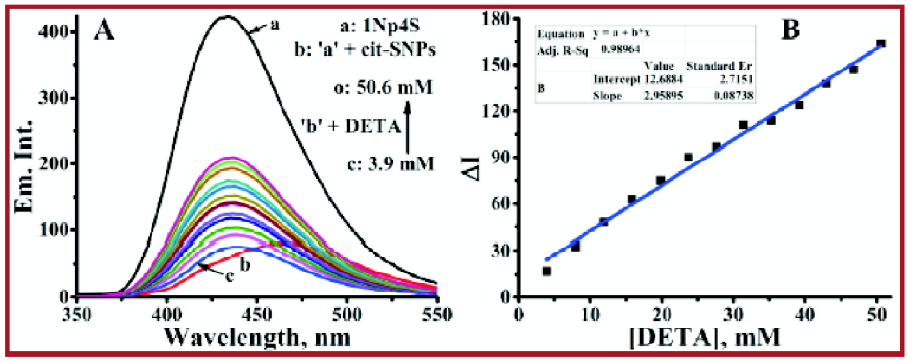

Fig. 6. (A) Emission spectra of (a) 1Np4S; (b) 'a' + cit-SNPs; (c-o) 'b' + DETA (3.9–50.6 mM); (B) calibration curve for DETA.

Evaluation of DETA:

In order to evaluate DETA concentration in an aqueous solution, as described in the preceding section, we have made a calibration curve of a plot of change of emission intensity (ΔI) vs concentration of DETA. The emission spectra of the 1Np4S functionalized cit-SNPs in the presence of DETA at various concentrations (3.9–50.6 mM) were recorded and are shown in Fig. 6A. The figure reveals that the emission intensity increases with increasing concentration of DETA. Like EDA, the particles' surface adsorbed 1Np4S in its deprotonated forms get associated with DETA through H-bonding (···HNH/NH···$^{-}$ ONpSO$_3^{-}$···); consequently, 1Np4S desorbs from the particles' surface and its emission intensity increases gradually. Calibration curve was constructed from a plot of change of emission intensity (ΔI) at 434 nm of 1Np4S functionalized cit-SNPs vs concentration of DETA and is shown in Fig. 6B. The ΔI value increases lineraly with the concentration of DETA. The data are well fit in a linear equation, ΔI = 12.6884 + 2.95895 [DETA] with adj. R^2 = 0.98964. The LOD and LOQ values are found to be 1.88 mM and 6.25 mM, respectively. All data are listed in Table S2.

Conclusions

We have studied photophysical property of 1Np4S and used it successfully for the functionalization of citrate stabilized silver nanoparticles (cit-SNPs). The functionalized particles were treated as fluorometric nanoprobe for the evaluation of two polyamines: ethylenediamine (EDA) and diethylenetriamine (DETA) from their aqueous solutions. As these two polyamines are mimicking of BGAs, thus, the 1Np4S functionalized cit-SNPs could be treated as potential nanoprobe for evaluating BGAs.

Acknowledgements

Authors are thankful to Department of Chemistry, NIT Agartala for providing research facilities and CRF, NIT

Agartala for TEM analysis. SAK and NBN are grateful to NIT Agartala for providing institutional fellowship received from MHRD, Govt. of India. SR is thankful to BRNS, DAE, Govt. of India, Sanction no. 36(4)/14/12/2018-BRNS/36235 for financial support.

Supporting Information

Supporting information includes results of Stern-Volmer plots (Table S1) and calibration curves of EDA and DETA (Table S2).

References

1. A. Asan and I. Isildak, *Mikrochim. Acta,* 1999, **132**, 13.
2. R. Paseiro-Cerrato, A. R. de Quirós, R. Sendón, J. Bustos, M. I. Santillana, J. M. Cruz and P. Paseiro-Losada, *Compr. Rev. Food Sci. Food Saf.*, 2010, **9**, 676.
3. D. D. Bills, K. I. Hildrum, R. A. Scanlan and L. M. Libbey, *J. Agric. Food Chem.*, 1973, **21**, 876.
4. K. I. Hildrum, R. A. Scanlan and L. M. Libbey, *J. Agric. Food Chem.*, 1975, **23**, 34.
5. J. H. Hotchkiss, R. A. Scanlan and L. M. Libbey, *J. Agric. Food Chem.*, 1977, **25**, 1183.
6. L. F. Bjeldanes, D. E. Schutz and M. M. Morris, *Food Cosmet. Toxicol.*, 1978, **16**, 157.
7. C. H. Chu and L. F. Bjeldanes, *J. Food Sci.*, 1981, **47**, 79.
8. J. Y. Hui and S. L. Taylor, *Toxicol. Appl. Pharmacol.*, 1985, **81**, 241.
9. H. Yamanaka, K. Shimakura, K. Shiomi, T. Kikuchi and M. Okuzumi, *J. Food Hyg. Soc. Jpn.*, 1987, **28**, 354.
10. C. Panaitescu, C. Jinescu, A. M. Mares, *Revista De Chimie,* 2016, **67**, 925.
11. A. Onal, *Food Chem.*, 2007, **103**, 1475-1486.
12. (a) M. H. S. Santos, *Int. J. Food Microbiol.*, 1996, **29**, 213; (b) A. R. Shalaby, *Food Res. Int.*, 1996, **29**, 675.
13. E. Agostinelli, M. P. M. Marques, R. Calheiros, F. P. S. C. Gil, G. Tempera, N. Viceconte, V. Battaglia, S. Grancara and A. Toninello, *Amino Acids*, 2010, **38**, 393.
14. M. L. Henriks-Eckerman and T. Laijoki, *J. Chromatogr.*, 1985, **333**, 220.
15. B. Paz-Pino, C. Pérez-Lamela, B. Cancho-Grande, J. Simal-Gándara, *Food Addit. Contam.,* 2003, **20**, 308.
16. K. Saito, M. Horie, N. Nose, K. Nakagomi and H. Nakazawa, *Anal. Sci.*, 1992, **8**, 675.
17. F. Crea, A. De Robertis and S. Sammartano, *J Chromatogr. Sci.*, 2007, **43**, 342.
18. R. Liu, K. Bi, Y. Jia, Q. Wang, R. Yin and Q. Li, *J. Mass Spectrom.,* 2012, **47**, 1341.
19. R. Westerholm, H. Li and J. Almen, *Chemosphere*, 1993, **27**, 1381.
20. S. Einarsson, B. Josefsson and S. Lagerkrist, *J. Chromatogr.*, 1983, **282**, 609.
21. S. Suzuki, K. Kobayashi, J. Nada, T. Suzuki and K. Takama, *J. Chromatogr.*, 1990, **508**, 225.
22. I. R. C. Whiteside, P. J. Worsfold and E. H. McKerrell, *Anal. Chim. Acta*, 1988, **212**, 155.
23. R. M. Danner, T. V. Reddy and C. W. Guion, *LC-GC*, 1994, **12**, 244.
24. H. Vuorela, P. Lehtonen and R. Hiltunen, *J. Liq. Chromatogr.*, 1991, **14**, 3181.
25. Y. Nishikawa and K. Kuwata, *Anal. Chem.*, 1984, **56**, 1790.
26. K. Anderson, C. Hallgren, J. D. Levin and C. A. Nilson, *J. Chromatogr.*, 1984, **312**, 482.
27. M.-L. Chen, Y.-Y. Feng, S.-Y. Wang, Y.-H. Cheng and Z.-H. Zhou, *ACS Appl. Mater. Interfaces*, 2020, **12**, 1412.
28. T. K. Misra and C. Y. Liu, *J. Colloid Interface Sci.*, 2008, **326**, 411.
29. T. K. Misra and C.-Y. Liu, *J. Nanopart. Res.*, 2009, **11**, 1053.
30. R. Choudhury, A. Purkayastha, D. Debnath and T. K. Misra, *J. Mol. Liq.,* 2017, **238**, 96.
31. R. Choudhury and T. K. Misra, *Colloids Surf. A*, 2018, **545**, 179-187.
32. S. A. Khan, R. Choudhury, M. Majumdar and T. K. Misra, *Spectrochim. Acta, Part A,* 2020, **234**, 118240.
33. Y. Chen, J. Zhang, Y. Gao, J. Lee, H. Chen and Y. Yin, *Biosens. Bioelectron.*, 2015, **72**, 306.
34. Y. Yao, Y. Zhou, J. Dai, S. Yue and M. Xue, *Chem. Commun.*, 2014, **50**, 869.
35. C. Han, L. Zeng, H. Li and G. Xie, *Sensor. Actuat. B: Chem.*, 2009, **137**, 704.
36. (a) T. Förster, *Naturwissen-schaften*, 1949, **36**, 186; (b) T. Förster, *Z. Elektrochem.*, 1950, **54**, 531.
37. O. Gajst, G. G. Rozenman and D. Huppert, *J. Phys. Chem. A*, 2018, **122**, 209.
38. A. S. I. Amer, A. M. M. Alazaly and A. A. Abdel-Shafi, *J. Photochem. Photobiol. A: Chem.*, 2019, **369**, 202.
39. S. S. Al-Shihry, *Spectrochim. Acta, Part A*, 2005, **61**, 2439.
40. R. Choudhury, A. Purkayastha, D. Debnath and T. K. Misra, *J. Mol. Recognit.,* 2016, **29**, 452.
41. D. D. Evanoff and G. Chumanov, *ChemPhysChem,* 2005, **6**, 1221.
42. M. Chanana and M. L.-M. Luis, *Nanophotonics*, 2012, **1**, 199.
43. U. Kreibig and M. Vollmer, "Optical Properties of Metal Clusters", Springer, 1995, Vol. 25.
44. R. M. C. Henson and P. A. H. Wyatt, *J. Chem. Soc., Faraday Trans. 2,* 1975, **71**, 669.
45. R. Krishnan, J. Lee and G. W. Robinson, *J. Phys. Chem.*,

1990, **94**, 6365.

46. L. M. Tolbert, K. M. Solntsev, *Acc. Chem. Res*., 2002, **35**, 19.
47. D. Mandal, S. K. Pal and K. Bhattacharyya, *J. Phys. Chem. A*, 1998, **102**, 9710.
48. A. Varlan and M. Hillebrand, *Molecules*, 2010, **15**, 3905.
49. M. R. Eftink and C. A. Ghiron, *J. Phys. Chem.*, 1976, **80**, 486.
50. J. Seetharamappa and B. P. Kamat, *Chem. Pharm. Bull.*, 2004, **52**, 1053.
51. M. Maciazek-Jurczyk, J. Rownicka-Zubik, R. Dyja and A. Sulkowska, *Acta Physica Polonica A*, 2013, **123**, 673.